Numerical Investigation of Slag Entrainment

This article presents a three-dimensional, transient, multi-phase, turbulent numerical model intended to predict slag entrainment in metallurgical systems such as continuous casting. Experiments report the critical angular velocity of the cylinder at which oil entrainment starts to occur, and the model reasonably agrees.

Mold slag entrainment, i.e., liquid mold powder being drawn into the melt, is a challenge in the production of clean steel. The literature identifies nine mechanisms[1,2] of mold slag entrainment, shown in Figure 1:

1. Top surface fluctuations.
2. Meniscus freezing/hook formation.
3. Vortex formation in the wake of the submerged entry nozzle (SEN).
4. Shear-layer instability.
5. Upward flow impinging upon the top surface.
6. Argon bubble interactions/slag foaming.
7. Slag crawling down the submerged entry nozzle.
8. Top surface stationary wave instability.
9. Top surface "balding."

Entrainment depends on the mass density (ρ), dynamic shear viscosity (μ) and interfacial tension (Γ) of the involved fluids. The orientation of the slag-steel interface relative to the direction of gravity also affects entrainment.

This work explores the "upward flow impinging upon the top surface" entrainment mechanism in an oil-water system. Metal producers need to be able to predict the onset of entrainment, to cause it during ladle treatment and to prevent it during casting as a function of process variables. The ultimate goal of this work is to relate the tendency for entrainment with, for example, casting conditions such as casting speed, argon gas flowrate, SEN design and operation, electromagnetic flow control design and operation, and mold dimensions.

Previous Studies of Slag Entrainment

The previous studies of slag entrainment have used analytical models, oil-water physical models and numerical models. These studies explored the critical speed V_{crit} at or near the liquid interface at which entrainment occurs; speeds in excess of this critical value result in slag entrainment. The numerical constants in the equations presented in this section expect that all quantities are given in m-kg-second units, i.e., mass density in

Figure 1

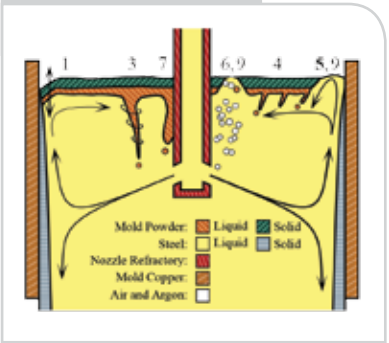

Slag entrainment mechanisms.[1,2]

Authors

Kenneth E. Swartz
graduate research assistant, Department of Mechanical Science and Engineering, The University of Illinois at Urbana-Champaign, Urbana, Illinois, USA
swartz6@illinois.edu

Lance C. Hibbeler
postdoctoral research associate, Department of Mechanical Science and Engineering, The University of Illinois at Urbana-Champaign, Urbana, Illinois, USA
lance.hibbeler@gmail.com

Brendan P. Joyce
quality assurance analyst, Schneider Electric, Chicago, Ill., USA
brendan.joyce@schneider-electric.com

Brian G. Thomas
C.J. Gauthier Professor of Mechanical Engineering, Department of Mechanical Science and Engineering, The University of Illinois at Urbana-Champaign, Urbana, Illinois, USA
bgthomas@illinois.edu

kg/m^3, dynamic shear viscosity in Pa·s, interfacial tension in N/m, and layer thickness in m, to give speed in m/second.

Analytical Models — Anlaytical expressions have been derived to predict the critical entrainment speed V_{crit} between two parallel-flowing, stratified fluids. An analysis of the stability of the interface,[3,4] shown in Figure 2, gives

$$\frac{V_{crit}}{\sqrt[4]{g\Gamma_{u\ell}/\rho_u}} = \sqrt[4]{4}\sqrt{1+\frac{\rho_u}{\rho_\ell}}\sqrt[4]{\frac{1}{\rho_u/\rho_\ell}-1} \quad \text{(Eq. 1)}$$

where

g = acceleration due to gravity and
u and ℓ = the upper fluid, i.e., oil or slag, and lower fluid, i.e., water or steel, respectively.

The speed necessary for instability depends on the size of the perturbation to the interface, and Equation 1 occurs at the critical wavelength $\lambda_c = 2\pi\sqrt{\Gamma_{u\ell}/g(\rho_\ell-\rho_u)}$, where the effects of interfacial tension and gravity are balanced. The analysis underlying Equation 1 assumed irrotational and inviscid fluids in an infinite domain; relaxing the latter two assumptions[5] gives Equation 2.

The critical speed predicted by Equation 2 is found by minimizing the equation with respect to λ, which occurs at about λ_c. This viscous model predicts a lower critical speed than the inviscid model, Equation 1, because of the momentum transport by shear stresses. Equation 2 shows that the upper layer acts infinitely thick when $h_u > 3\lambda_c/2\pi$, or about 27 mm for oil-water systems and 15 mm for steel-slag sytems, which suggests that ladle systems are not sensitive to the layer thickness. The phenomenon illustrated in Figure 2 has long been under investigation; many other theoretical and experimental treatments[6–8] are found in the literature.

Figure 2

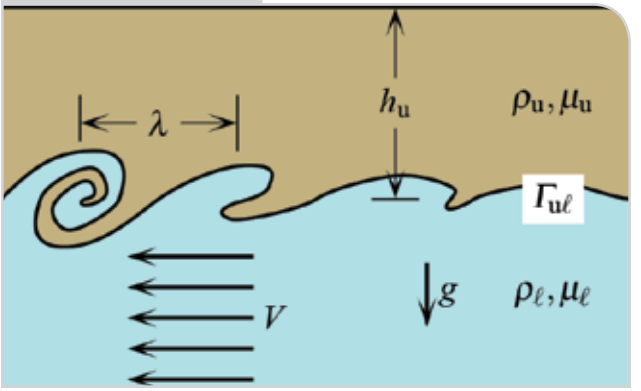

Shear instability analytical model.[3–5]

One model proposed that entrainment occurs when the kinetic energy of a spherical droplet, E_K, exceeds the sum of the energy cost of forming the surface area, E_S, and the work done by the buoyancy force through a distance of one-half of the droplet diameter, W_B, i.e., the work done to pull a droplet out of the slag layer.[9] The critical entrainment speed predicted by this model is:

$$\frac{V_{crit}}{\sqrt[4]{g\Gamma_{u\ell}/\rho_u}} = \sqrt[4]{48}\sqrt[4]{\frac{1}{\rho_u/\rho_\ell}-1} \quad \text{(Eq. 3)}$$

A similar analysis based on forces[10,11] instead of energies predicts that the critical entrainment speed is:

Equation 2

$$v_{instability}(\lambda) = \sqrt{\left(g(\rho_\ell-\rho_u)\frac{\lambda}{2\pi}+\Gamma_{u\ell}\frac{2\pi}{\lambda}\right)\frac{\left(\mu_\ell+\mu_u\coth\left(\frac{2\pi}{\lambda}h_u\right)\right)^2}{\left(\rho_u\coth\left(\frac{2\pi}{\lambda}h_u\right)\right)\mu_\ell^2+\rho_\ell\left(\mu_u\coth\left(\frac{2\pi}{\lambda}h_u\right)\right)^2}}$$

where

h_u = the thickness of the upper fluid layer and
μ = the dynamic shear viscosity.

$$\frac{V_{crit}}{\sqrt[4]{g\Gamma_{u\ell}/\rho_u}} = \sqrt[4]{\frac{128}{3}\cos(\varphi)}\sqrt[4]{\frac{1}{\rho_u/\rho_\ell}-1}$$

(Eq. 4)

where φ = the angle of the liquid interface relative to the direction of gravity, as shown in Figure 3.

The critical speed from Equation 4 always is less than that from Equation 3. For a horizontal interface, i.e., φ = 90°, the critical speed from Equation 4 is zero, which indicates some error in the model.

Oil-Water Physical Models — One experimental apparatus used a submerged hose that was aimed at a vertical wall in a rectangular tank,[12,13] shown in Figure 4. Measurements were made using laser-image velocimetry (LIV). The original results[12] from the hose apparatus were reduced to the expression:

$$V_{crit} = c\frac{\Gamma_{u\ell}^{1.037}}{g^{0.012}}\frac{(\rho_\ell-\rho_u)^{0.239}}{\rho_u^{0.227}}\frac{\mu_u^{0.321}}{\mu_\ell^{1.370}}$$

(Eq. 5)

where $c = 1.2 \times 10^{-3}$ is a dimensionless constant.

An extended study[13] with the hose apparatus produced the expression:

$$V_{crit} = c\frac{\Gamma_{u\ell}^{0.292}g^{0.115}}{h_u^{0.365}}\frac{(\rho_\ell-\rho_u)^{0.215}}{\rho_u^{0.694}}\frac{\mu_u^{0.231}}{\mu_\ell^{0.043}}$$

(Eq. 6)

where $c = 3.065$ is a dimensionless constant.

Another experimental apparatus used a submerged rotating cylinder in a rectangular tank,[14,15] shown in Figure 5. The measured critical speeds were reduced to a critical capillary number Ca = $\mu V/\Gamma\Gamma$as a function of the ratio of kinematic shear viscosities ν_u/ν_ℓ. An early study[14] measured the tangential velocity of the surface of the cylinder and proposed the expression:

$$V_{crit} = c_1\frac{\Gamma_{u\ell}}{\mu_\ell}\exp\left(c_2\frac{\nu_u}{\nu_\ell}\right)$$

(Eq. 7)

Figure 3

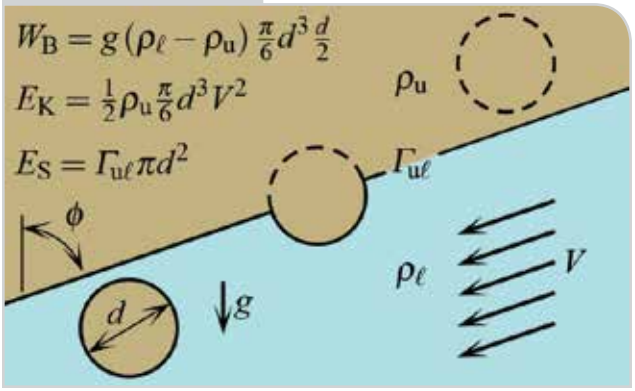

Droplet entrainment analytical model.[9–11]

Figure 4

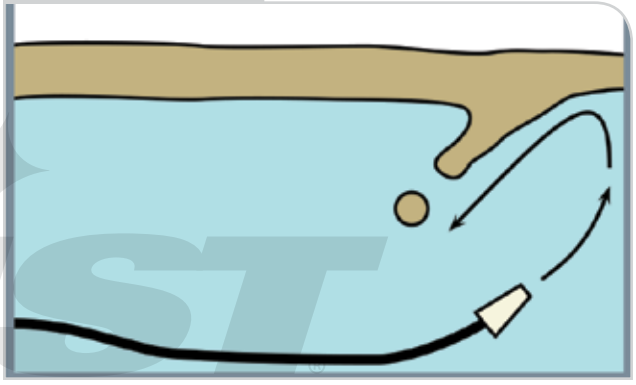

Hose apparatus.[12,13]

where

ν = μ/ρ is the kinematic shear viscosity,
$c_1 = 0.0233$ is a dimensionless constant and
$c_2 = 0.001$ is a dimensionless constant.

Because Equation 7 gives very large speeds, a later study[15] used particle-image velocimetry (PIV) to measure the water speed 2 mm away from the surface of the cylinder and proposed the expression:

$$V_{crit} = \frac{\Gamma_{u\ell}}{\mu_\ell}\left(c_1 + c_2\frac{\nu_u}{\nu_\ell}\right)$$

(Eq. 8)

where

$c_1 = 2.8 \times 10^{-3}$ is a dimensionless constant and
$c_2 = 3 \times 10^{-6}$ is a dimensionless constant.

Figure 5

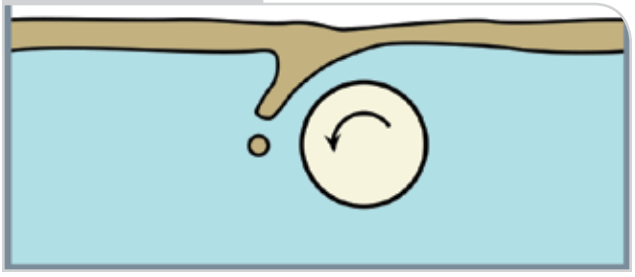

Cylinder apparatus.[14,15]

Figure 6

Ramp apparatus.[16]

Figure 7

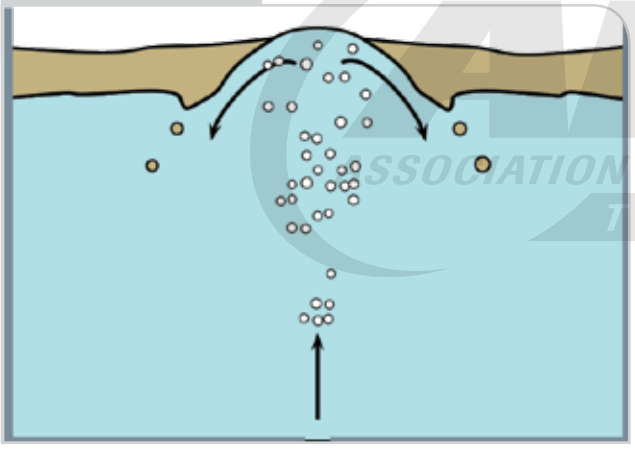

Ladle-like apparatus.[11,18–21]

Figure 8

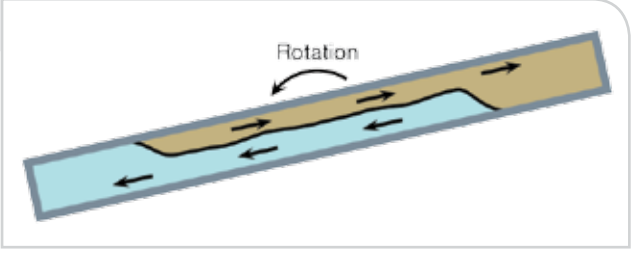

Rotating trough apparatus.[6–8,22]

Another study used a ramp/weir submerged in a rectangular tank,[16] shown in Figure 6. Measurements were made with PIV. These researchers did not propose an expression for critical entrainment speed, but did explore a wide range of properties.

Gas-stirred ladles have flow phenomena similar to molds that cause entrainment. In ladles, entrainment often is desirable because of the increase in slag-steel interfacial area and corresponding increase in mass transfer during stirring. The main difference between entrainment in a ladle and in a mold, from a fluid-mechanic perspective, is that ladle slag layers are about 10 times thicker than mold slag layers. Many studies of ladles have explored a critical gas flowrate.[10,11,17] Because of various difficulties with velocimetry in round vessels, other studies used a rectangular ladle-like apparatus,[11,18–21] shown in Figure 7, to explore the critical interface speed. One study[21] with laser-Doppler velocimetry (LDV) measured a critical entrainment speed of 0.233 m/second, and the researchers proposed, based on this single data point, that entrainment occurs at a Weber number $We = \rho V_{crit}^{\,2} L/\Gamma_{u\ell}$ of 12.3, using the lower-fluid mass density and characteristic length of $L = \lambda_c/2\pi$, which gives the critical entrainment speed as:

$$V_{crit} = \sqrt[4]{151.3\Gamma_{u\ell}\frac{g(\rho_\ell - \rho_u)}{\rho_\ell^2}} \qquad \text{(Eq. 9)}$$

Another study with a similar ladle-like apparatus[18–20] measured with PIV a critical entrainment speed of 0.264 m/second. The oil speeds near the interface were observed[18–20] to be about one-tenth as much as the speeds in the water. Another study[11] supported the predictions of Equation 4 and its accompanying droplet size model at speeds greater than the critical.

The shear instability phenomenon shown in Figure 2 has been explored experimentally by using a rotating trough,[6,7,8,22] as shown in Figure 8. These experiments offer controllable conditions to investigate the behavior of the fluid interface, but the finiteness of the domain limits the applicability of the measurements in metallurgical processes.

Numerical Models — The shear-layer instability shown in Figure 2 was investigated for a slag-steel system with a temperature gradient through the slag layer and temperature-dependent properties.[1] This investigation observed degrees of instability of the interface, i.e., that the interface can be considered unstable without entraining droplets, and found that slag entrainment occurred at about 1.1 m/second.

Three-dimensional (3D) large-eddy simulations[23,24] of the flow in the ramp apparatus shown in Figure 6 explored the entrained droplet creation rate[24] and size distribution.[23,24] The two-phase model[24] used both oil-water and slag-steel systems, and the three-phase model[23] used air, oil and water. These models underpredict the experimentally observed[16] droplet diameters by a factor of 2 or more, but indicate that the droplet size distribution is insensitive to the fluid-system material properties.

An axisymmetric, argon-slag-steel multi-phase numerical model of heat transfer and turbulent fluid flow in a ladle[25] supports Equation 9. A 2D oil-water multi-phase numerical model of turbulent fluid flow in the ladle-like apparatus[18,26] shown in Figure 7 predicts[18] a critical entrainment speed of (0.24 ±0.02) m/second, which agrees with the (0.26 ±0.04) m/second that was measured[18–20] in the apparatus. However, this simulation used an eddy viscosity model specialized for jets and not a general-purpose turbulence model.

Comparison and Evaluation of Previous Work — The quantitative agreement of the models in the literature is poor. Using the material properties listed in Table 1, the critical entrainment speeds predicted by the models discussed in this section are presented in Table 2. If needed, the upper-layer thickness is h_u = 10 mm and the angle of the interface from gravity is $\varphi = 60°$. The predicted entrainment speeds vary widely, particularly in the slag-steel system, though the property values are reasonable; these models should be applied carefully outside of the conditions for which they were developed. The disagreement among models can be explained by differences in interface geometry, the sensitivity of the phenomenon to interfacial tension and measurement technique. Additionally, the observation that the fluid in the upper layer is not at rest[18–20] affects the reliability of the theoretical model predictions.

Figure 9 evaluates eight of the models presented in this section with the available measurements. The measurements from the ramp apparatus[16] perhaps are subject to some systematic error. The theoretical models are as accurate as could be expected, and the empirical models work well only for the measurements to which they were fit. Fitting measurements against a single dimensionless number, e.g., Equations 7–9, or a product of several dimensionless numbers, e.g., Equations 5 and 6, oversimplifies the problem and sheds little light on the underlying physics of entrainment. Dimensionless quantities like the Weber number are intended to be used as order-of-magnitude quantifications of flow regimes. Empirical models may be used for plant practice, but the scatter presented in Figure 9 casts reasonable doubt on all of the models reviewed in this section. Across all the data, Equation 6 seems to be the best fit with an error of about ±25%.

Qualitatively, the previous experimental studies are in good agreement. The critical entrainment speed has been observed:

- To increase with increasing $\Gamma_{u\ell}$.[12,13,16]
- To increase with increasing difference in density between the ρ_u and ρ_ℓ.[12,13,16]

Table 1

Typical Values of Fluid-System Properties Used in Literature Model Comparisons

System	Mass density			Dynamic shear viscosity			Kinematic shear viscosity			Interfacial tension	Characteristic velocity	Capillary wavelength
	ρ_u (kg/m^3)	ρ_ℓ (kg/m^3)	ρ_u/ρ_ℓ	μ_u (mPa·s)	μ_ℓ (mPa·s)	μ_u/μ_ℓ	ν_u (mm^2/s)	ν_ℓ (mm^2/s)	ν_u/ν_ℓ	$\Gamma_{u\ell}$ mN/m	$\sqrt[4]{g\Gamma_{u\ell}/\rho_u}$ m/s	λ_c mm
Oil-water	960	997	0.963	50	0.9	50	52.1	1.00	52.0	30	0.132	56.4
Slag-steel	2,500	7,200	0.347	300	5	60	120	0.694	173	1,100	0.256	30.7

Table 2

Literature Model Predictions of Critical Entrainment Speed in m/second

System	Theoretical models				Experimental models				
	Eq. 1[3,4]	Eq. 2[5]	Eq. 3[9]	Eq. 4[11]	Eq. 5[12]	Eq. 6[13]	Eq. 7[14]	Eq. 8[15]	Eq. 9[21]
Oil-water	0.116	0.0825	0.154	0.126	0.0873	0.0963	0.823	0.0991	0.620
Slag-steel	0.493	0.254	0.790	0.645	1.59	0.565	6.09	0.730	0.202

Figure 9

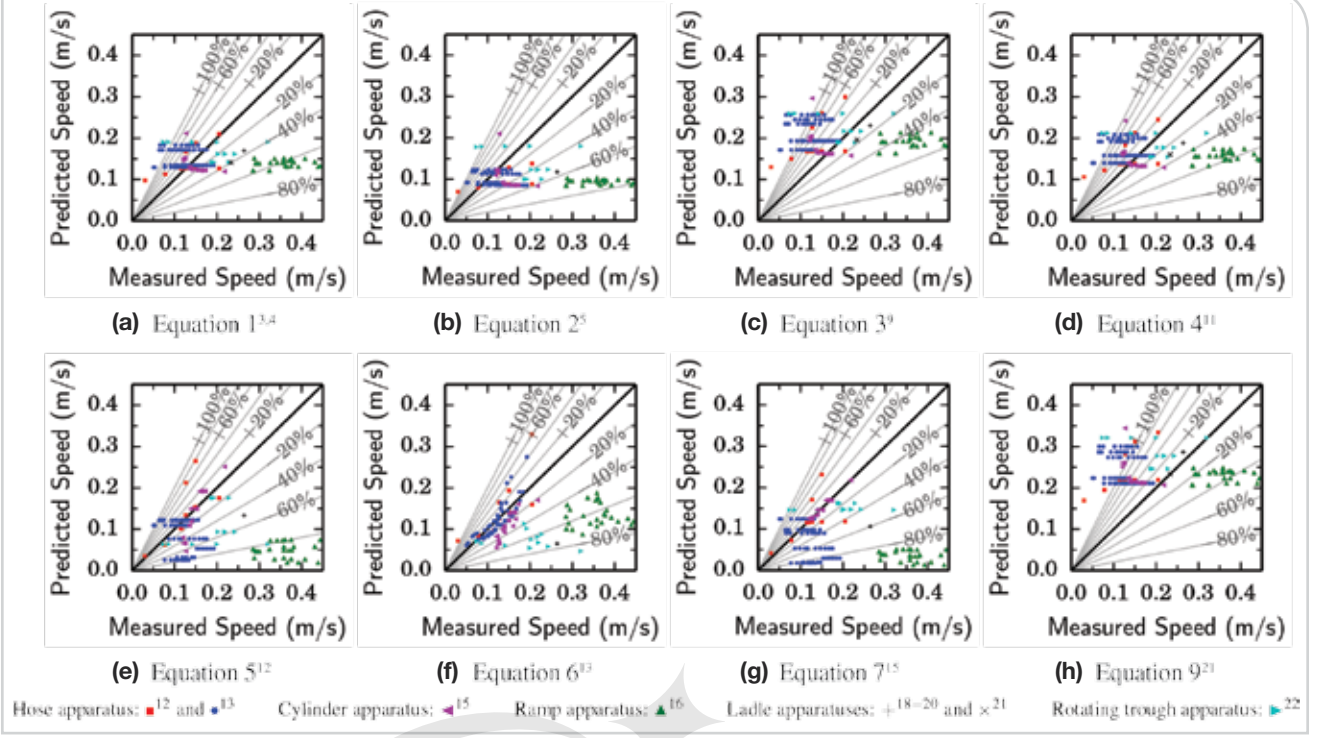

Evaluation of literature models for available data.

- To increase with increasing ratio of ν_u/ν_ℓ.[14,15,17]
- To increase with increasing μ_u.[12,13,15,16]
- To increase with,[16] to decrease with[13,17] and to be independent of[15] h_u.

However, in experiments it is difficult to change independently each material property. The diameter of the entrained droplets has been observed:

- To increase with increasing $\Gamma_{u\ell}$.[12,15,16]
- To increase with decreasing difference in density between the ρ_u and ρ_ℓ.[12,16]
- To increase with increasing ratio of ν_u/ν_ℓ.[14,15]
- To increase with increasing μ_u.[12,16]
- To increase with[16] and to be independent of[13] h_u.

Most researchers[11–13,16,17] measure the diameter of the entrained oil droplets in the range of 5–10 mm, but others[15] have reported diameters as large as 30 mm. Quantitative knowledge of droplet size is useful for calculating post-entrainment droplet behavior in molds and ladles and for predicting the enhancement to mass transfer during stirring in ladles.

The inviscid energetic model, Equation 3, intuitively is an upper bound for entrainment, which is of little practical use. The theoretical models suggest that λ_c and $\sqrt[4]{g\Gamma_{u\ell}/\rho_u}$ are the characteristic length and speed for interfacial phenomena; the characteristic time then is $\lambda_c/\sqrt[4]{g\Gamma_{u\ell}/\rho_u}$, which may be useful in predicting entrained droplet formation rates. Analysis of experimental data demonstrated that measurements scale well with this characteristic speed.[17] Though the functional relationship remains to be determined, the best course of action seems to be a fit of the form:

$$\frac{V_{crit}}{\sqrt[4]{g\Gamma_{u\ell}/\rho_u}} = f\left(\frac{\rho_u}{\rho_\ell}, \frac{h_u}{\lambda_c}, \mu_u, \mu_\ell, \varphi\right) \quad \text{(Eq. 10)}$$

where $f = 0$ at ρ_u/ρ_ℓ, and the dependence of f on h_u/λ_c should monotonically and asymptotically tend toward "no effect" as h_u/λ_c increases. In any case, future work on this subject should report the complete data set $\{V_{crit}, \rho_u, \rho_\ell, \mu_u, \mu_\ell, \Gamma_{u\ell}, h_u, \phi\}$ for each measurement. Given the stochastic nature of the phenomenon, any future effort also must include enough repeated measurements so that sound statistical conclusions may be drawn.

Description of Numerical Model of Slag Entrainment

The slag entrainment phenomenon is explored in this work with a numerical model because in-situ investigations are prohibitively difficult and previous work is lacking. The analytical treatments simplify the physics for the sake of achieving a closed-form solution, and oil-water physical models do not satisfy all of the necessary similarity criteria and are subject to experimental variability. Numerical modeling offers precise control over the physics and boundary conditions, and omniscient knowledge of the state of the system, though the technique is not without its shortcomings, such as turbulence modeling and mesh resolution.

This work uses a transient, multi-phase, turbulent numerical model to explore entrainment phenomena, implemented with the commercial software FLUENT.[27] The model solves the Navier-Stokes equations for the mixture and one volume-fraction weighted continuity equation for the upper fluid. The shear-stress transport (SST) k-ω model[28] is employed to model the effects of turbulence in the fluid mixture with low Reynolds number correction factors and additional damping for the fluid interfaces, with a damping factor of 10. Multi-phase phenomena are treated with the volume-of-fluid (VOF) method,[29] with surface tension effects treated with the continuum surface force (CSF) method.[30] Further details are described elsewhere.[27]

The governing equations are discretized with the finite volume method (FVM) and then are solved on a fixed, unstructured grid. In the momentum, turbulent kinetic energy and turbulent dissipation rate equations, the advective terms are discretized with the second-order upwind scheme, and the diffusive terms are discretized with the second-order central scheme. Velocities and turbulence quantities are modeled at cell centers, and pressure is modeled at cell-face centers; this staggering* of the pressure computes pressure gradients more accurately than co-locating the pressure and velocity, particularly at boundaries. Cell-face quantities, namely the flux quantities, are computed as the face-average value of the quantity at the nodes, which are computed from weighted averages of the values in the surrounding cells.†

The volume fraction equations are discretized with the explicit geometric-reconstruction scheme,[31] generalized for unstructured meshes.[27] This method was found to be more accurate and less diffuse than other methods.[32] Pressure-velocity coupling is treated with the pressure-implicit splitting of operators (PISO) method[33] using a single neighbor-correction iteration. Using the PISO method allows the under-relaxation factors for the pressure, momentum and turbulence equations to be taken as unity. The reference pressure in the pressure-correction equation is taken as 101325 Pa and is located at $\boldsymbol{x}^{\mathrm{ref}}$. Transient simulations are solved using first-order, non-iterative time advancement. The time step is determined during the simulation by keeping the largest Courant number $||\boldsymbol{v}||/(\Delta x/\Delta t)$ less than some maximum value $C_{\max}$.

Model Verification

Model verification evaluates programming/implementation fidelity by comparing the solution computed by the numerical model with an analytical solution of a simple test problem. Verification also allows easy exploration of appropriate time steps, mesh sizes and other model parameters. Two test problems are employed in this work to verify the numerical model. A single-phase verification problem considers long, concentric rotating cylinders at steady state, or "tangential annular drag flow." This test problem demonstrates that the model can accurately relate pressure gradients, shear stresses and velocities. A multi-phase test problem, "two-fluid rotating cylinder," considers air and water in an axially rotating cylinder to verify that the model can accurately track a fluid interface. An important finding from the two-fluid rotating cylinder test problem was that geometric-reconstruction discretization of the volume-fraction equations ensures that the fluid interface is three cells wide regardless of mesh size. This finding is key to interpreting the model validation results: to fully resolve the dynamics of a droplet of diameter d requires cell sizes of about $d/10$. For larger cells, the model is computing the average behavior of a fluid mixture, and

* In FLUENT, this method is referred to as the pressure staggering option, or the PRESTO method. This method is a generalization to unstructured meshes of the staggered pressure technique found in textbooks on computational fluid dynamics.

† In FLUENT, this method is referred to as the Green–Gauss node-based method for gradient quantities. This approach has been demonstrated to be more accurate for unstructured meshes than the usual approach of taking the arithmetic mean of adjacent cell-center values.[27]

Figure 10

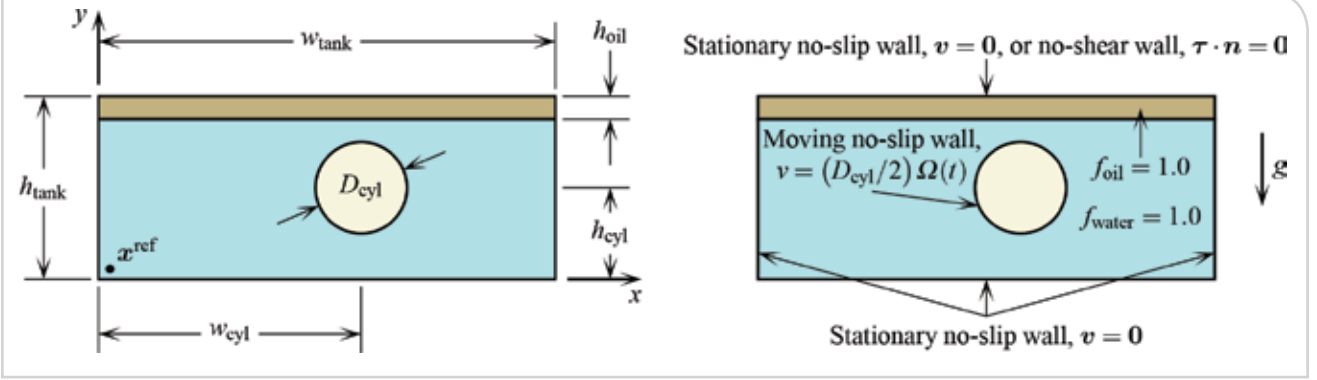

Domain, boundary and initial conditions for model validation simulations.

Figure 11

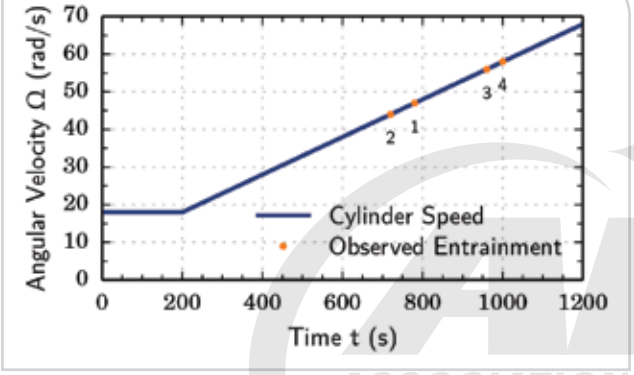

Angular velocity of cylinder.

Table 3

Conditions for Model Validation Simulations

Quantity	Symbol	Value	Unit
Tank width	w_{tank}	200	mm
Tank height	h_{tank}	80	mm
Tank thickness	t_{tank}	60	mm
Cylinder horizontal position	w_{cyl}	115	mm
Cylinder vertical position	h_{cyl}	40	mm
Cylinder diameter	D_{cyl}	40	mm
Oil layer thickness	h_{oil}	10	mm
Acceleration due to gravity	g	9.807	m/s^2
Maximum Courant number	C_{max}	0.4	—
Reference pressure location	x^{ref}	(1,1,1)	mm

nothing can be claimed about surface interactions with the droplet. However, the diameter of the oil droplet within a cell volume V_{cell} can be estimated as:

$$d = \sqrt[3]{(6/\pi) f_{oil} V_{cell}} \qquad \text{(Eq. 11)}$$

which is consistent with the VOF method used to model the multi-phase phenomena. Detailed conditions and results of both test problems can be found in the full version of this text.[32]

Model Validation

Model validation evaluates the ability of the model to duplicate experimental measurements. Validation ensures that the numerical model contains appropriate physics and boundary conditions. The numerical model used in this work is validated in this section with data from the cylinder apparatus[15] shown in Figure 5. The most reliable data from that experimental study are the angular velocities of the cylinder at the onset of entrainment, hereafter called the "critical angular velocities," which are used in this work as the validation targets.

Oil-Water Model Description — The domain and boundary conditions in the numerical model, shown in Figure 10, mirror the experiments. The domain is a 3D rectangular tank with an axially rotating cylinder inside of it. A layer of oil rests on top of a bath of water, and the cylinder rotates with increasing angular velocity to induce entrainment. The domain is discretized with 102,360 hexahedral cells, with an edge length of about 2 mm and cell volume of V_{cell} = 8.7 mm^3. The problem conditions are summarized in Table 3, and the properties for the four oils used in this work are given in Table 4. The 3D simulations in this work were computed on a 6-core, 2.67 GHz workstation and required about one week per simulation.

The top wall boundary condition is either a no-slip wall, i.e., a closed tank, to simulate a solid powder layer, or a no-shear wall, i.e., an open tank, to simulate a free surface. The experimentalists reported insignificant differences in entrainment behavior between the two top wall conditions.[15]

The angular velocity of the cylinder is prescribed as:

$$\Omega(t) = \begin{cases} \Omega_0 & \text{if } 0 \le t \le t_0 \\ \Omega_0 + \alpha\left(t - t_0\right) & \text{if } t_0 \le t \end{cases}$$

(Eq. 12)

where Ω = 18 rad/second is the angular velocity applied for t_0 = 200 seconds to establish an initial steady state. From this steady state, the cylinder is accelerated with angular acceleration α = 0.05 rad/second^2 until entrainment occurs. The angular velocity evolution is plotted in Figure 11. The experimentalists found[15] that entrainment behavior is independent of angular acceleration for α = 0.05 rad/second^2. In the numerical model, the time-dependent velocity of the cylinder surface is applied with a FLUENT user-defined function as:

$$v_x = -(D_{cyl}/2)\,\Omega\sin(\theta)$$

(Eq. 13)

$$v_y = (D_{cyl}/2)\,\Omega\cos(\theta)$$

(Eq. 14)

$$v_z = 0$$

(Eq. 15)

with Ω calculated from Equation 12 and the angle θ calculated from the coordinates of a point on the surface of the cylinder as:

$$\theta = \text{atan2}(y - h_{cyl},\ x - w_{cyl})$$

(Eq. 16)

Oil-Water Model Results — The initial validation efforts simulated a 2D slice through the center of the tank. An entrained "droplet" in two dimensions is a cylinder, so the interfacial tension was taken as zero to cancel this error. Entraining a cylinder is more difficult than entraining a sphere because of the larger surface area, and the previous work discussed in the literature review showed that entrainment is easier with lower interfacial tension. Under these conditions, for Oil 2, the simulated critical angular velocity overpredicts the measurement by 6.5% for a no-slip top wall. If interfacial tension is included in the 2D simulation, entrainment does not occur for a no-slip top wall boundary condition, and for a no-shear top wall the simulated critical angular velocity overpredicts the measurement by 0.15%. With interfacial tension and a no-slip top wall boundary condition, the simulated oil layer broke into two distinct sections, which was not observed in the experiments.[15]

The 3D simulations are in good agreement with the experimental measurements for the lower-viscosity oils, as shown in Table 5. The oil layer in the simulations broke apart at about x = 160 mm; although the layer did not break in the experiments,[15] the simulation results still are valid near the cylinder. The volume of water increased by 6.59 x 10^{-5}% over the simulation.

The critical angular velocities reported in Table 5 were determined by examining the behavior of the iso-surface. Using Equation 11, this value of oil volume-fraction with cells 2 mm on a side corresponds to an oil droplet diameter of about 1 mm. According to the mesh study performed on the two-fluid rotating cylinder verfication problem, this mesh can resolve droplets of about 20-mm diameter.

For Oil 2, using a no-slip top wall and the described entrainment criterion, the model underpredicts the measured critical angular velocity by about 4%. The critical entrainment speed, measured 3.5 mm from

Table 4

Fluid Properties From the Cylinder Apparatus Experiments[15]

	Mass density		Dynamic shear viscosity		Kinematic shear viscosity		Interfacial tension
Fluid	ρ (kg/m^3)	ρ_u/ρ_ℓ	μ (mPa·s)	μ_u/μ_ℓ	ν (mm^2/s)	ν_u/ν_ℓ	$\Gamma_{u\ell}$ (mN/m)
Water	997	—	0.9	—	0.903	—	—
Oil 1	920	0.923	4.6	5.1	5.0	5.5	40
Oil 2	930	0.933	9.3	10	10	11	40
Oil 3	963	0.966	96.0	107	99.7	110	42
Oil 4	966	0.969	193	214	200	221	44

Figure 12

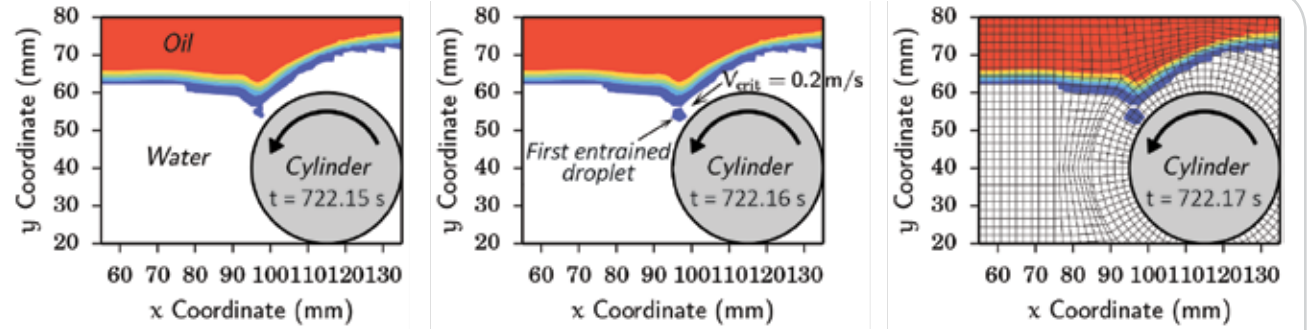

Section view of validation domain at z = 36.5 mm, showing Oil 2 entrainment at Ω = 44.1 rad/second.

the f_{oil} = 0.5 iso-surface, is 0.2 m/second, which is comparable to values reported in the literature review. Figure 12 shows a 2D slice of the f_{oil} contours from 0.01 to 1.00 at z = 36.5 mm relative to the back face of the tank. This figure looks similar to the photographs of the experiments[15] shown in Figure 13. These photographs are for an oil with ν_u/ν_ℓ = 50, while the simulated oil in Figure 12 has ν_u/ν_ℓ = 10. The simulations calculate that the droplet formation occurs over 0.1 second, while the experimentalists[15] report about 4 seconds; other experimental work[18–20,26] reports about 0.3 second for the droplet formation time. Figure 14 shows an end view with the same conditions as Figure 12, with the f_{oil} = 0.03 iso-surface shown for clarity. Both of these figures show a fingerlike protrusion from the oil layer immediately prior to droplet formation; this behavior was observed in almost all of the cited previous experimental studies. In Figure 14, the brightly colored region is the oil touching the wall, and the shaded region is the perspective view of the deformed oil-water interface. Repeating the simulation with a no-shear top wall underpredicts the measured critical angular velocity by about 9%.

The critical angular velocities reported in Table 5 correspond to the first entrained droplet that is not in contact with the cylinder or the walls. Droplets were entrained at and moved along the walls at lower angular velocities than the reported values, but these droplets are considered as numerical artifacts because of the assumption of a wetting angle of 90° and the coarse mesh. These erroneous droplets accumulate in the lower corners of the tank, as shown in Figure 14. Future modeling work should resolve these issues by including a realistic wetting angle and a more refined mesh near the walls.

The simulations of Oils 3 and 4, as well as an oil with ν_u/ν_ℓ = 50, do not match the experiments. The oil layer breaks into two sections, leaving no oil within about one D_{cyl} of the center of the cylinder, which is denoted with * in Table 5. The no-shear top wall boundary condition has not been simulated for Oil 4 because the same result is expected. When the oil-water interface comes too close to the top wall, the oil suddenly spreads farther apart. This behavior is caused by an assumed wetting angle of 90°, which is employed due to a lack of wetting angle measurements for the fluids used in this work. This error could be corrected by refining the mesh or using a three-phase model with a layer of air on top of the oil to remove this boundary effect. Future modeling work should explore why the model, as it stands, cannot correctly simulate the behavior of the most viscous oil.

Table 5

Measured and Calculated Critical Cylinder Angular Velocities in rad/second

	Closed tank (no-slip top wall)		Open tank (no-shear top wall)	
Fluid	Measured	Calculated	Measured	Calculated
Oil 1	46±2	48	47±2	43
Oil 2	46±2	44	44±2	40
Oil 3	53±2	*	56±3	*
Oil 4	59±1	*	58±1	—

*Oil layer broke into two distinct sections

Conclusions

A three-dimensional, transient, two-phase numerical model of turbulent fluid flow has been developed for oil-water or slag-steel systems to predict entrainment. The model uses the geometric-reconstruction volume-of-fluid (VOF) scheme with the shear-stress transport (SST) k-ω turbulence model in FLUENT. The VOF results with a coarse mesh should be interpreted appropriately by looking at low volume fraction iso-surfaces. The model has been verified with the analytical solutions of laminar tangential annular

Figure 13

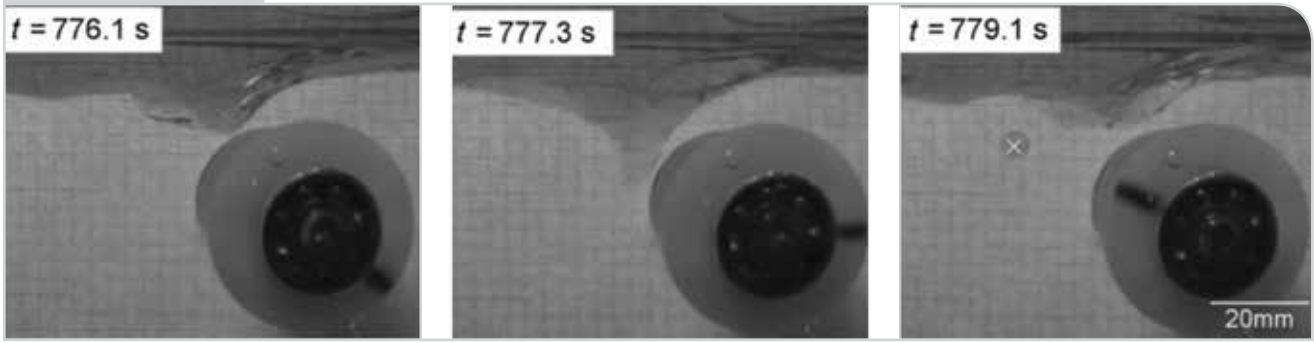

Photographs of entrainment experiments (from Figure 5 of Reference 15).

drag flow and the shape of the air-water interface in an axially rotating cylinder. The model has been validated with experiments of oil entrainment into water caused by a rotating cylinder: the 3D model matches the measured values to within 4% or 9%, depending on the boundary condition on the top of the oil layer. However, more work is recommended to improve the model-predicted behavior regarding breakup of the interface, especially for more-viscous oils. This model is ready to apply in the investigation of slag entrainment in metallurgical systems, with appropriate properties for the slag and steel.

Acknowledgments

The financial support of the members of the Continuous Casting Consortium at the University of Illinois at Urbana-Champaign (UIUC) is acknowledged gratefully. At the time of writing, the members are: ABB, ArcelorMittal, Baosteel, Magnesita Refractories, Nippon Steel and Sumitomo Metal Corp., Nucor Steel Decatur, POSTECH/POSCO, Severstal, SSAB, Tata Steel and ANSYS-FLUENT. The authors also thank Professor S.P. Vanka at UIUC and Dr. Rui Liu at ArcelorMittal Global Research and Development for helpful discussions about the numerical simulations in this work.

References

1. L.C. Hibbeler, R. Liu and B.G. Thomas, "Review of Mold Flux Entrainment Mechanisms and Model Investigation of Entrainment by Shear-Layer Instability," *Proceedings of the 7th European Continuous Casting Conference,* Steel Institute VDEh, 2011.

Figure 14

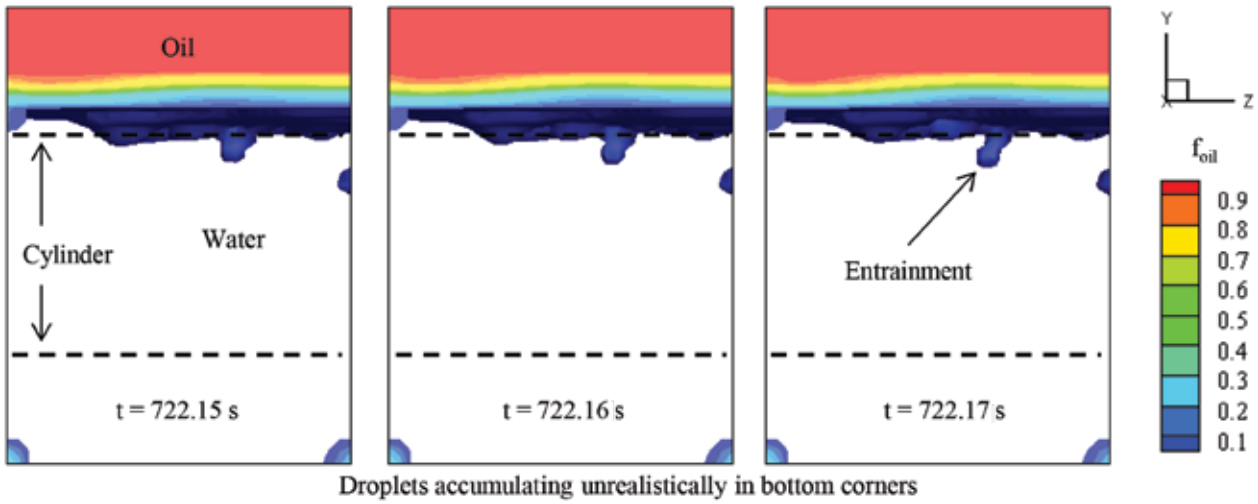

End view of validation domain from x = 0, showing Oil 2 entrainment at Ω = 44.1 rad/second.

2. L.C. Hibbeler and B.G. Thomas, "Mold Slag Entrainment Mechanisms in Continuous Casting Molds," *Iron & Steel Technology,* Vol. 8, No. 10, 2013, pp. 121–136.
3. H.L.F. von Helmholtz, "On Discontinuous Movement of Fluids (in German)," *Monthly Reports of the Royal Prussian Academy of Sciences in Berlin,* Vol. 23, 1868, pp. 215–228.
4. W. Thomson, "Hydrokinetic Solutions and Observations," *Philosophical Magazine,* Vol. 42, No. 281, 1871, pp. 362–377.
5. T. Funada and D.D. Joseph, "Viscous Potential Flow Analysis of Kelvin–Helmholtz Instability in a Channel," *Journal of Fluid Mechanics,* Vol. 445, 2001, pp. 263–283.
6. S.A. Thorpe, "On Standing Internal Gravity Waves of Finite Amplitude," *Journal of Fluid Mechanics,* Vol. 32, No. 3, 1968, pp. 489–528.
7. S.A. Thorpe, "Experiments on the Instability of Stratified Shear Flows: Immiscible Fluids," *Journal of Fluid Mechanics,* Vol. 39, No. 1, 1969, pp. 25–48.
8. S.A. Thorpe, "Experiments on the Instability of Stratified Shear Flows: Miscible Fluids," *Journal of Fluid Mechanics,* Vol. 46, No. 2, 1971, pp. 299–319.
9. S. Asai, "Fluid Flow and Mass Transfer in Metallurgical Processes Where Stirring Is Utilized," *Proceedings of the 100th and 101st Nishiyama Memorial Lecture,* The Iron and Steel Institute of Japan, 1984, pp. 65–100.
10. J. Mietz, S. Schneider and F. Oeters, "Emulsification and Mass Transfer in Ladle Metallurgy," *Steel Research,* Vol. 62, No. 1, 1991, pp. 10–15.
11. T. Wei and F. Oeters, "A Model Test for Emulsion in Gas-Stirred Ladles," *Steel Research,* Vol. 63, No. 2, 1992, pp. 60–68.
12. S.L. Feldbauer, "Slag Entrainment in the Mold of a Continuous Caster," Ph.D. thesis, Carnegie Mellon University, 1995.
13. J.M. Harman and A.W. Cramb, "A Study of the Effect of Fluid Physical Properties Upon Droplet Emulsification," *79th Steelmaking Conference Proceedings,* Iron & Steel Society, 1996, pp. 773–784.
14. P.R. Scheller and R. Hagemann, "Model Investigations on Slag Entrainment in Continuous Casting," *Archives of Metallurgy and Materials,* Vol. 57, No. 1, 2012, pp. 283–289.
15. R. Hagemann, R. Schwarze, H.P. Heller and P.R. Scheller, "Model Investigations on the Stability of the Steel-Slag Interface in Continuous Casting Process," *Metallurgical and Materials Transactions B,* Vol. 44, No. 1, 2013, pp. 80–90.
16. J. Savolainen, T. Fabritius and O. Mattila, "Effect of Fluid Physical Properties on the Emulsification," *ISIJ International,* Vol. 49, No. 1, 2009, pp. 29–36.
17. M. Iguchi, Y. Sumida, R. Okada and Z-I. Morita, "Evaluation of Critical Gas Flowrate for the entrApment of Slag Using a Water Model," *ISIJ International,* Vol. 34, No. 2, 1994, pp. 164–170.
18. K. Krishnapisharody, "Model Studies on Fluid Mechanic Interactions Between Steel and Slag in Gas-Stirred Ladles," Ph.D. thesis, McMaster University, 2007.
19. K. Krishnapisharody and G.A. Irons, "Model Studies on Slag Droplet Generation in Gas-Stirred Ladles," *EPD Congress 2008, Proceedings of The Minerals, Metals, and Materials Society 138th Annual Meeting,* The Minerals, Metals and Materials Society, 2008, pp. 293–302.
20. K. Krishnapisharody and G.A. Irons, "Modeling and Analysis of Slag Droplet Formation in Ladle Metallurgy Practice," *AISTech 2008 Conference Proceedings,* Vol. II, 2008, pp. 1243–1252.
21. Z. Xiao, Y. Peng and C. Liu, "Modeling Study of the Entrapment Phenomena at the Slag-Metal Interface in the Gas-Stirred Ladle," *Chinese Journal of Metal Science and Technology,* Vol. 3, No. 4, 1987, pp. 187–193.
22. M. Iguchi, J. Yoshida, T. Shimizu and Y. Mizuno, "Model Study on the Entrapment of Mold Powder Into Molten Steel," *ISIJ International,* Vol. 40, No. 7, 2000, pp. 685–691.
23. P. Sulasalmi, A. Kärnä, T. Fabritius and J. Savolainen, "CFD Model for Emulsification of Slag Into the Steel," *ISIJ International,* Vol. 49, No. 11, 2009, pp. 1661–1667.
24. A. Senguttuvan and G.A. Irons, "Model Studies on Slag Metal Entrainment in Gas-Stirred Ladles," *AISTech 2013 Conference Proceedings,* Vol. I, 2013, pp. 1231–1241.
25. L. Jonsson and P. Jönsson, "Modeling of Fluid Flow Conditions Around the Slag/Metal Interface in a Gas-Stirred Ladle," *ISIJ International,* Vol. 36, No. 9, 1996, pp. 1127–1134.
26. K. Krishnapisharody and G.A. Irons, "Numerical Simulation of Droplet Generation of the Buoyant Phase in Two-Phase Liquid Baths," *EPD Congress 2008, Proceedings of The Minerals, Metals and Materials Society 138th Annual Meeting,* The Minerals, Metals and Materials Society, 2008, pp. 311–322.
27. ANSYS Inc., *ANSYS FLUENT 14 Theory Guide,* 2011.
28. F.R. Menter, "Two-Equation Eddy-Viscosity Turbulence Models for Engineering Applications," *AIAA Journal,* Vol. 32, No. 8, 1994, pp. 1598–1605.
29. C.W. Hirt and B.D. Nichols, "Volume of Fluid (VOF) Method for the Dynamics of Free Boundaries," *Journal of Computational Physics,* Vol. 39, No. 1, 1981, pp. 201–225.
30. J.U. Brackbill, D.B. Kothe and C. Zemach, "A Continuum Method for Modeling Surface Tension," *Journal of Computational Physics,* Vol. 100, No. 2, 1992, pp. 335–354.
31. D.L. Youngs, "Time-Dependent Multi-Material Flow With Large Fluid Distortion," *Numerical Methods for Fluid Dynamics,* K.W. Morton and M.J. Baines, eds., No. 24, New York: Academic Press, 1982, pp. 273–285.
32. K.E. Swartz, L.C. Hibbeler, B.P. Joyce and B.G. Thomas, "Numerical Investigation of Slag Entrainment," *AISTech 2014 Conference Proceedings,* Vol. II, 2014, pp. 1865–1879.
33. R.I. Issa, "Solution of the Implicitly Discretized Fluid Flow Equations by Operator Splitting," *Journal of Computational Physics,* Vol. 62, No. 1, 1986, pp. 40–65. ✦

The original version of this paper was presented at AISTech 2014 — The Iron & Steel Technology Conference and Exposition, Indianapolis, Ind., and published in the Conference Proceedings.